fractal and fractional

MDPI

Article

An Eighth-Order Numerical Method for Spatial Variable-Coefficient Time-Fractional Convection–Diffusion–Reaction Equations

Yuelong Feng [1], Xindong Zhang [2,*] and Leilei Wei [3]

[1] School of Mathematical Sciences, Xinjiang Normal University, Urumqi 830017, China; fyl001215@163.com
[2] College of Big Data Statistics, Guizhou University of Finance and Economics, Guiyang 550025, China
[3] School of Mathematics and Statistics, Henan University of Technology, Zhengzhou 450001, China; leileiwei@haut.edu.cn
* Correspondence: liaoyuan1126@163.com; Tel.: +86-1399-913-7720

Abstract

In this paper, we propose a high-order compact difference scheme for a class of time-fractional convection–diffusion–reaction equations (CDREs) with variable coefficients. Using the Lagrange polynomial interpolation formula for the time-fractional derivative and a compact finite difference approximation for the spatial derivative, we establish an unconditionally stable compact difference method. The stability and convergence properties of the method are rigorously analyzed using the Fourier method. The convergence order of our discrete scheme is $\mathcal{O}(\tau^{4-\alpha} + h^8)$, where τ and h represent the time step size and space step size, respectively. This work contributes to providing a better understanding of the dependability of the method by thoroughly examining convergence and conducting an error analysis. Numerical examples demonstrate the applicability, accuracy, and efficiency of the suggested technique, supplemented by comparisons with previous research.

Keywords: time-fractional CDREs; variable coefficients; compact difference method; Caputo fractional derivative; high-order convergence

check for updates

Academic Editor: Riccardo Caponetto

Received: 18 June 2025
Revised: 4 July 2025
Accepted: 7 July 2025
Published: 9 July 2025

Citation: Feng, Y.; Zhang, X.; Wei, L. An Eighth-Order Numerical Method for Spatial Variable-Coefficient Time-Fractional Convection–Diffusion–Reaction Equations. *Fractal Fract.* **2025**, *9*, 451. https://doi.org/10.3390/fractalfract9070451

Copyright: © 2025 by the authors. Licensee MDPI, Basel, Switzerland. This article is an open access article distributed under the terms and conditions of the Creative Commons Attribution (CC BY) license (https://creativecommons.org/licenses/by/4.0/).

1. Introduction

In the realm of contemporary scientific research and engineering applications, mathematical models are indispensable, with partial differential equations serving as a cornerstone. These equations are capable of effectively capturing the essential characteristics of dynamic behaviors in various systems, ranging from natural phenomena to engineering optimization. However, as the complexity of research subjects continues to grow, traditional integer-order partial differential equations are increasingly insufficient. This limitation has driven researchers to explore new mathematical frameworks to meet these challenges.

Fractional calculus has emerged as a promising solution to address these limitations. Fractional differential equations, by incorporating fractional-order derivatives, can naturally describe systems with memory effects, non-local characteristics, and complex dynamics. This makes them a more flexible tool for modeling. Among the various fractional models, fractional CDREs have garnered significant attention due to their wide applicability across multiple fields. These equations are capable of describing the transport of substances in complex media and effectively characterizing reaction kinetics. This makes them highly valuable in areas such as environmental science [1,2], materials science [3,4], and biomedical engineering [5,6].

Nevertheless, solving fractional CDREs presents formidable challenges. The non-local nature of fractional derivatives, combined with potential nonlinear terms and variable coefficients in the equations, renders traditional numerical methods largely inadequate for efficiently solving these equations. Among the numerical methods for constant-coefficient cases, one can refer to the adaptive moving mesh method [7], finite element method [8–10], finite volume method [11], and finite difference method [12,13]. In contrast, the more practically significant variable-coefficient cases have received relatively little attention. The presence of variable coefficients complicates the physical properties of the equations and poses greater difficulties for the design and analysis of numerical methods. In recent years, scholars have made significant strides in addressing these challenges. In 2021, Li and Wang [14] developed numerical methods for time-fractional CDREs. They utilized finite differences for the Caputo fractional derivative and the local discontinuous Galerkin method for the spatial derivative. In 2022, Ngondiep [15] introduced an advanced two-level fourth-order numerical scheme designed for time-fractional CDREs with variable coefficients. This scheme demonstrated unconditional stability and achieved a convergence rate of $\mathcal{O}(\tau^{2-\frac{\alpha}{2}} + h^4)$. In 2023, Roul and Rohil [16] introduced a numerical method for multi-term time-fractional CDREs. It employs a graded mesh for the Liouville–Caputo fractional derivative and a compact finite difference method for spatial derivatives. Additionally, Hosseini et al. [17] proposed a meshless Generalized Finite Difference Method for nonlinear fractional CDREs. This approach leverages Taylor series and Moving Least Squares for spatial derivatives, ensuring reliability across complex domains. In 2024, Priyadarshana and Mohapatra [18] devised a numerical algorithm for 2D time-delayed parabolic CDREs. It utilizes an operator-splitting method and an upwind scheme on a Shishkin mesh. The Thomas algorithm is applied for computation efficiency, achieving first-order accuracy. Furthermore, Kumar et al. [19] presented a weak Galerkin finite-element method for singularly perturbed CDREs. This approach ensures higher-order convergence rates and is applicable to various polygonal mesh types, achieving $\mathcal{O}(h^k)$ in the triple-bar norm and $\mathcal{O}(h^{k+1})$ in the L^2 norm, where k represents the highest degree of the polynomials employed. In 2025, Liu et al. [20] proposed a high-order compact finite difference method for CDREs with variable exponents and coefficients. They used a space–time transformation and interpolation quadrature rule to handle the complexities. The aforementioned research results provide reliable references for numerical methods of fractional differential equations, but the convergence rates in both the time and space directions need further improvement. Inspired by the above research, this paper builds upon the studies of previous scholars and enhances the convergence rates of the algorithm in both the time and space directions, with convergence of the $4-\alpha$ order in time and the eighth order in space.

In the present work, we consider more general time-fractional CDREs with variable coefficients in order to better model complex physical phenomena [21].

$$\begin{cases} {}_0^C D_t^\alpha v(x,t) = d\dfrac{\partial^2 v}{\partial x^2}(x,t) - p_1(x)\dfrac{\partial v}{\partial x}(x,t) + p_2(x)v(x,t) + f(x,t), \\ v(0,t) = \varphi_1(t), \quad v(L,t) = \varphi_2(t), \\ v(x,0) = \varphi_3(x), \end{cases} \tag{1}$$

where $(x,t) \in (0,L) \times (0,T]$, d is the constant diffusion coefficient, p_1 and p_2 are variable coefficients dependent on x, and $f(x,t)$ represents external influences. The boundary conditions are $\varphi_1(t)$ at $x = 0$ and $\varphi_2(t)$ at $x = L$, and the initial condition is $\varphi_3(x)$. All

functions are assumed smooth enough to ensure the validity of the analysis. The Caputo fractional derivative ${}_0^C D_t^\alpha$ is defined as

$$ {}_0^C D_t^\alpha u(t) = \frac{1}{\Gamma(1-\alpha)} \int_0^t u'(s)(t-s)^{-\alpha} ds, \quad 0 < \alpha < 1. $$

To address the complexities of solving variable-coefficient time-fractional CDREs, this paper presents a novel numerical approach. This approach leverages the Lagrange polynomial interpolation formula for the time-fractional derivative and a compact finite difference approximation for the spatial derivative. This method not only achieves unconditional stability but also attains convergence rates of the $4-\alpha$ order in time and the eighth order in space, as rigorously analyzed through the Fourier method. By effectively addressing the challenges posed by variable coefficients, the proposed scheme significantly enhances numerical accuracy while maintaining computational efficiency. Three numerical experiments further validate the theoretical analysis, demonstrating superior performance compared to existing methods. This work thus offers a robust and efficient solution strategy for time-fractional CDREs, providing valuable support for modeling and analyzing complex systems in various fields.

This paper is organized as follows: Section 2 introduces the necessary mathematical notations and preliminary lemmas that form the foundation for developing our high-order compact finite difference scheme; Section 3 is dedicated to analyzing the stability and convergence properties of the proposed methods; Section 4 presents three numerical experiments that illustrate the practical application and effectiveness of our approach; and we conclude this paper with a summary of our findings and potential directions for future research in Section 5.

2. Construction of Full Discrete Scheme

To facilitate the analysis of Equation (1), we apply a series of transformations. These transformations are designed to address the challenges associated with variable coefficients and to simplify the equation by converting it into a more tractable form. Initially, we assume that the coefficient $p_1(x)$ is differentiable on the interval $[0, L]$ and define the following notations:

$$ u(x,t) = k(x)v(x,t), \quad g(x,t) = k(x)f(x,t), $$
$$ k(x) = \exp\Big(-\frac{1}{2d}\int_0^x p_1(s)ds\Big), \quad q(x) = p_2(x) + \frac{1}{2}\Big(\frac{dp_1}{dx} - \frac{p_1^2}{2d}\Big). $$

By addressing these complexities, Equation (1) is transformed into a more tractable form:

$$ \begin{cases} {}_0^C D_t^\alpha u(x,t) = d\dfrac{\partial^2 u}{\partial x^2}(x,t) + q(x)u(x,t) + g(x,t), & x \in (0,L), t \in (0,T], \\ u(0,t) = \phi_1(t), \quad u(L,t) = \phi_2(t), & t \in [0,T], \\ u(x,0) = \phi_3(x), & x \in [0,L], \end{cases} \tag{2} $$

where $\phi_1(t)$, $\phi_2(t)$, and $\phi_3(x)$ are assumed to be sufficiently smooth. Clearly, $v(x,t)$ is a solution of Equation (1) if and only if $u(x,t)$ satisfies Equation (2). Consequently, the remainder of our study is dedicated to Equation (2).

To construct a high-precision compact finite difference scheme for Equation (2), we define M and N as the numbers of spatial and temporal subdivisions, respectively, and $h = \frac{L}{M}$ and $\tau = \frac{T}{N}$ as the spatial and temporal step sizes. Let $[M] = \{1, 2, \cdots, M\}$. We define

$u_j^n = u(x_j, t_n)$ and $g_j^n = g(x_j, t_n)$, where x_j and t_n are the spatial and temporal grid points. The difference operators are defined as follows:

$$\delta_x^2 u_j = u_{j+1} - 2u_j + u_{j-1}, \quad \mathcal{L} = \frac{1}{h^2}\Big(1 + \frac{1}{560}\delta_x^6\Big)^{-1}\delta_x^2\Big(1 - \frac{1}{12}\delta_x^2 + \frac{1}{90}\delta_x^4\Big).$$

Here, we introduce several lemmas that are employed in the subsequent construction of the finite difference scheme.

Lemma 1 ([22]). *For the difference operator $\mathcal{L}$, it holds that $u_{xx}(x_j, t_n) = \mathcal{L}u_j^n + \mathcal{O}(h^8)$.*

Lemma 2 ([23]). *The discretized form of the Caputo derivative on a uniform mesh is given by*

$$\begin{aligned} {}_0^C D_t^\alpha u_j^n &= \frac{1}{\Gamma(1-\alpha)}\Big[\int_{t_0}^{t_1}(t_n - s)^{-\alpha}u'(s)\,ds + \int_{t_1}^{t_2}(t_n - s)^{-\alpha}u'(s)\,ds \\ &\quad + \sum_{k=3}^{n}\int_{t_{k-1}}^{t_k}(t_n - s)^{-\alpha}u'(s)\,ds\Big] \\ &= \frac{1}{\Gamma(2-\alpha)}\sum_{k=0}^{n}\lambda_k u_j^{n-k} + \mathcal{O}(\tau^{4-\alpha}). \end{aligned}$$

Here, the coefficients λ_k are consistent with those reported in Reference [23].

Lemma 3 ([23]). *Let λ_k be defined as $\tau^{-\alpha}\psi_k$. The coefficients ψ_k exhibit the following properties:*
(i) For $n \geq 3$ and any α in the interval $(0,1)$:
(i-1) ψ_0 is calculated as $\frac{1}{3} + \frac{1}{2-\alpha} + \frac{1}{(2-\alpha)(3-\alpha)}$, and it falls within the range $\Big(1, \frac{11}{6}\Big)$.
(i-2) ψ_2 is positive.
(i-3) ψ_k is negative for $k \geq 1$ and $k \neq 2$.
(ii) For any order $\alpha \in (0,1)$ and for all n, the sum of coefficients equals zero, i.e., $\sum_{k=0}^{n}\psi_k = 0$.

Now, using Lemmas 1 and 2, Equation (2) can be rewritten as

$$\frac{1}{\Gamma(2-\alpha)}\sum_{k=0}^{n}\lambda_k u_j^{n-k} = d\mathcal{L}u_j^n + q_j u_j^n + g_j^n + \mathcal{O}(\tau^{4-\alpha} + h^8). \tag{3}$$

By denoting U_j^n as the numerical estimate of u_j^n and omitting the truncation errors $\mathcal{O}(\tau^{4-\alpha} + h^8)$ in Equation (3), we obtain

$$\frac{1}{\Gamma(2-\alpha)}\sum_{k=0}^{n}\lambda_k U_j^{n-k} = d\mathcal{L}U_j^n + q_j U_j^n + g_j^n. \tag{4}$$

By multiplying both sides of Equation (4) by $1 + \frac{1}{560}\delta_x^6$ and introducing the parameters $\mu = \frac{1}{\Gamma(2-\alpha)}$ and $\theta = \frac{d}{h^2}$, we obtain the final discrete formulation

$$\begin{aligned} &\Big(\frac{\mu\lambda_0}{560} - \frac{q_j}{560} - \frac{\theta}{90}\Big)U_{j+3}^n + \Big(-\frac{3\mu\lambda_0}{280} + \frac{3q_j}{280} + \frac{3\theta}{20}\Big)U_{j+2}^n + \Big(\frac{3\mu\lambda_0}{112} - \frac{3q_j}{112} - \frac{3\theta}{2}\Big)U_{j+1}^n \\ &+ \Big(\frac{27\mu\lambda_0}{28} - \frac{27q_j}{28} + \frac{49\theta}{18}\Big)U_j^n + \Big(\frac{3\mu\lambda_0}{112} - \frac{3q_j}{112} - \frac{3\theta}{2}\Big)U_{j-1}^n \\ &+ \Big(-\frac{3\mu\lambda_0}{280} + \frac{3q_j}{280} + \frac{3\theta}{20}\Big)U_{j-2}^n + \Big(\frac{\mu\lambda_0}{560} - \frac{q_j}{560} - \frac{\theta}{90}\Big)U_{j-3}^n \\ &= +\Big(\frac{1}{560}g_{j+3}^n - \frac{3}{280}g_{j+2}^n + \frac{3}{112}g_{j+1}^n + \frac{27}{28}g_j^n + \frac{3}{112}g_{j-1}^n - \frac{3}{280}g_{j-2}^n + \frac{1}{560}g_{j-3}^n\Big) \\ &\quad - \mu\sum_{k=1}^{n}\lambda_k\Big(\frac{1}{560}U_{j+3}^{n-k} - \frac{3}{280}U_{j+2}^{n-k} + \frac{3}{112}U_{j+1}^{n-k} + \frac{27}{28}U_j^{n-k} + \frac{3}{112}U_{j-1}^{n-k} \\ &\quad - \frac{3}{280}U_{j-2}^{n-k} + \frac{1}{560}U_{j-3}^{n-k}\Big), \end{aligned} \tag{5}$$

with the initial and boundary conditions

$$U_j^0 = \widetilde{\phi}_3(x_j), \quad \text{and} \quad U_0^n = \widetilde{\phi}_1(t_n) = \widetilde{\phi}_1^n \quad \text{and} \quad U_M^n = \widetilde{\phi}_2(t_n) = \widetilde{\phi}_2^n.$$

For the computation of ghost-point values, we utilize the extrapolation formulas presented below:

$$\begin{aligned}
U_{-2}^k &= 36U_0^k - 168U_1^k + 378U_2^k - 504U_3^k + 420U_4^k - 216U_5^k + 63U_6^k - 8U_7^k + \mathcal{O}(h^8),\\
U_{-1}^k &= 8U_0^k - 28U_1^k + 56U_2^k - 70U_3^k + 56U_4^k - 28U_5^k + 8U_6^k - U_7^k + \mathcal{O}(h^8),\\
U_{M+1}^k &= 8U_M^k - 28U_{M-1}^k + 56U_{M-2}^k - 70U_{M-3}^k + 56U_{M-4}^k - 28U_{M-5}^k + 8U_{M-6}^k\\
&\quad - U_{M-7}^k + \mathcal{O}(h^8),\\
U_{M+2}^k &= 36U_M^k - 168U_{M-1}^k + 378U_{M-2}^k - 504U_{M-3}^k + 420U_{M-4}^k - 216U_{M-5}^k\\
&\quad + 63U_{M-6}^k - 8U_{M-7}^k + \mathcal{O}(h^8).
\end{aligned}$$

3. Stability and Convergence Analyses

In this section, we conduct a comprehensive theoretical analysis to establish the stability and convergence of the proposed numerical method for solving time-fractional CDREs with variable coefficients.

3.1. Stability Analysis

In this subsection, let $\widehat{U}_j^n$ represent the approximate solution of Equation (5). We define the error term as

$$\varepsilon_j^n = \widehat{U}_j^n - U_j^n, \quad j \in [M-1], n \in [N].$$

Consequently, we have

$$\begin{aligned}
&\Big(\frac{\mu\lambda_0}{560} - \frac{q_j}{560} - \frac{\theta}{90}\Big)\varepsilon_{j+3}^n + \Big(-\frac{3\mu\lambda_0}{280} + \frac{3q_j}{280} + \frac{3\theta}{20}\Big)\varepsilon_{j+2}^n + \Big(\frac{3\mu\lambda_0}{112} - \frac{3q_j}{112} - \frac{3\theta}{2}\Big)\varepsilon_{j+1}^n\\
&+ \Big(\frac{27\mu\lambda_0}{28} - \frac{27q_j}{28} + \frac{49\theta}{18}\Big)\varepsilon_j^n + \Big(\frac{3\mu\lambda_0}{112} - \frac{3q_j}{112} - \frac{3\theta}{2}\Big)\varepsilon_{j-1}^n\\
&+ \Big(-\frac{3\mu\lambda_0}{280} + \frac{3q_j}{280} + \frac{3\theta}{20}\Big)\varepsilon_{j-2}^n + \Big(\frac{\mu\lambda_0}{560} - \frac{q_j}{560} - \frac{\theta}{90}\Big)\varepsilon_{j-3}^n\\
&= -\mu\sum_{k=1}^{n}\lambda_k\Big(\frac{1}{560}\varepsilon_{j+3}^{n-k} - \frac{3}{280}\varepsilon_{j+2}^{n-k} + \frac{3}{112}\varepsilon_{j+1}^{n-k} + \frac{27}{28}\varepsilon_j^{n-k}\\
&\quad + \frac{3}{112}\varepsilon_{j-1}^{n-k} - \frac{3}{280}\varepsilon_{j-2}^{n-k} + \frac{1}{560}\varepsilon_{j-3}^{n-k}\Big).
\end{aligned} \tag{6}$$

The Fourier series representation of $\varepsilon^n(x)$ and its associated coefficients are given by

$$\varepsilon^n(x) = \sum_{l=-\infty}^{\infty}\xi_n(l)e^{i\beta x}, \quad \text{where} \quad \xi_n(l) = \frac{1}{L}\int_0^L \varepsilon^n(x)e^{-i\beta x}dx, \quad \beta = \frac{2\pi l}{L} \quad \text{and} \quad i = \sqrt{-1}.$$

By leveraging the definition of the L^2 norm and invoking Parseval's theorem, we derive

$$\|\varepsilon^n\|^2 = h\sum_{i=1}^{M-1}|\varepsilon_i^n|^2 = \int_0^L |\varepsilon_i^n|^2 dx \quad \text{and} \quad \int_0^L |\varepsilon^n(x)|^2 dx = L\sum_{l=-\infty}^{\infty}|\xi_n(l)|^2,$$

and, thus, we have

$$\|\varepsilon^n\|^2 = L\sum_{l=-\infty}^{\infty}|\xi_n(l)|^2. \tag{7}$$

We make the Fourier series assumption for $\varepsilon_j^n = \xi_n e^{i\beta jh}$, and we substitute it into Equation (6). After simplification, we obtain

$$\begin{aligned}&\xi_n\Big[\Big(\frac{\mu\lambda_0}{280}-\frac{q_j}{280}-\frac{\theta}{45}\Big)\cos(3\beta h)+\Big(-\frac{3\mu\lambda_0}{140}+\frac{3q_j}{140}+\frac{3\theta}{10}\Big)\cos(2\beta h)\\&+\Big(\frac{3\mu\lambda_0}{56}-\frac{3q_j}{56}-3\theta\Big)\cos(\beta h)+\Big(\frac{27\mu\lambda_0}{28}-\frac{27q_j}{28}+\frac{49\theta}{18}\Big)\Big]\\&=-\mu\sum_{k=1}^{n}\lambda_k\Big(\frac{1}{280}\cos(3\beta h)-\frac{3}{140}\cos(2\beta h)+\frac{3}{56}\cos(\beta h)+\frac{27}{28}\Big)\xi_{n-k}.\end{aligned}\tag{8}$$

From Equation (8), it follows that ξ_n can be written as

$$\xi_n=\sum_{k=1}^{n}\frac{-\mu\lambda_k B_1}{(\mu\lambda_0-q_j)B_1+\theta B_2}\xi_{n-k},\tag{9}$$

where B_1 and B_2 are defined as follows:

$$\begin{aligned}B_1&=\frac{1}{70}\Big(\cos^3(\beta h)-3\cos^2(\beta h)+3\cos(\beta h)+69\Big),\\B_2&=-\frac{4}{45}\Big(\cos^3(\beta h)-\frac{27}{4}\cos^2(\beta h)+\frac{132}{4}\cos(\beta h)-\frac{109}{4}\Big).\end{aligned}$$

We use C to represent various positive, bounded constants that may differ from one case to another.

Theorem 1. *The numerical scheme given by Equation (5) is unconditionally stable for* $\alpha \in (0,1)$.

Proof. First, we apply mathematical induction to prove that

$$|\xi_n| \le C|\xi_0|, \quad n \in [N].$$

When $n = 1$, according to Equation (9), we have

$$|\xi_1|=\Big|\frac{-\mu\lambda_1 B_1}{(\mu\lambda_0-q_j)B_1+\theta B_2}\xi_0\Big|\le\Big|\frac{\mu\lambda_0 B_1}{(\mu\lambda_0-q_j)B_1+\theta B_2}\Big||\xi_0|,\tag{10}$$

where $\lambda_1 = -\lambda_0$ (refer to Kumari et al. [23] for details). Given that

$$\mu=\frac{1}{\Gamma(2-\alpha)},\quad \theta=\frac{d}{h^2},\quad B_1>0,\quad B_2\ge 0,$$

and that the function

$$q(x)=p_2(x)+\frac{1}{2}\Big(\frac{dp_1}{dx}-\frac{p_1^2}{2d}\Big),$$

is bounded, we have

$$|\xi_1| \le C|\xi_0|.$$

Next, we assume that the inequality

$$|\xi_n| \le C|\xi_0|$$

holds for $n = 2, 3, \cdots, N-1$.

When $n = N$, according to Equation (9) and Lemma 3, we have

$$\begin{aligned}|\xi_N| &= \Big|\sum_{k=1}^{N} \frac{-\mu\lambda_k B_1}{(\mu\lambda_0 - q_j)B_1 + \theta B_2}\xi_{N-k}\Big| \\ &\le \sum_{k=1}^{N} \Big|\frac{-\mu\lambda_k B_1}{(\mu\lambda_0 - q_j)B_1 + \theta B_2}\Big||\xi_{N-k}| \\ &\le \sum_{k=1}^{N} |\psi_k|\Big|\frac{-\mu\tau^{-\alpha} B_1}{(\mu\tau^{-\alpha}\psi_0 - q_j)B_1 + \theta B_2}\Big|C|\xi_0| \\ &\le C(\psi_0 + 2\psi_2)|\xi_0| \\ &\le C|\xi_0|.\end{aligned} \tag{11}$$

By Equations (7) and (11), we obtain

$$\begin{aligned}\|\varepsilon^n\|^2 &= L\sum_{l=-\infty}^{\infty} |\xi_n(l)|^2 \\ &\le L\sum_{l=-\infty}^{\infty} C^2|\xi_0(l)|^2 \\ &= C^2\|\varepsilon^0\|^2.\end{aligned}$$

Therefore, the numerical scheme given by Equation (5) is unconditionally stable. □

3.2. Convergence Analysis

In this subsection, we discuss the convergence of Equation (5). In a similar manner, let

$$E_j^n = u_j^n - U_j^n, \quad j \in [M-1], n \in [N].$$

By subtracting Equation (4) from Equation (3) and noting that $E_j^0 = 0$, we can establish the following:

$$\begin{aligned}&\Big(\frac{\mu\lambda_0}{560} - \frac{q_j}{560} - \frac{\theta}{90}\Big)E_{j+3}^n + \Big(-\frac{3\mu\lambda_0}{280} + \frac{3q_j}{280} + \frac{3\theta}{20}\Big)E_{j+2}^n + \Big(\frac{3\mu\lambda_0}{112} - \frac{3q_j}{112} - \frac{3\theta}{2}\Big)E_{j+1}^n \\ &+ \Big(\frac{27\mu\lambda_0}{28} - \frac{27q_j}{28} + \frac{49\theta}{18}\Big)E_j^n + \Big(\frac{3\mu\lambda_0}{112} - \frac{3q_j}{112} - \frac{3\theta}{2}\Big)E_{j-1}^n \\ &+ \Big(-\frac{3\mu\lambda_0}{280} + \frac{3q_j}{280} + \frac{3\theta}{20}\Big)E_{j-2}^n + \Big(\frac{\mu\lambda_0}{560} - \frac{q_j}{560} - \frac{\theta}{90}\Big)E_{j-3}^n \\ &= +\Big(\frac{1}{560}R_{j+3}^n - \frac{3}{280}R_{j+2}^n + \frac{3}{112}R_{j+1}^n + \frac{27}{28}R_j^n + \frac{3}{112}R_{j-1}^n - \frac{3}{280}R_{j-2}^n + \frac{1}{560}R_{j-3}^n\Big) \\ &\quad - \mu\sum_{k=1}^{n-1}\lambda_k\Big(\frac{1}{560}E_{j+3}^{n-k} - \frac{3}{280}E_{j+2}^{n-k} + \frac{3}{112}E_{j+1}^{n-k} + \frac{27}{28}E_j^{n-k} + \frac{3}{112}E_{j-1}^{n-k} \\ &\quad - \frac{3}{280}E_{j-2}^{n-k} + \frac{1}{560}E_{j-3}^{n-k}\Big)\end{aligned} \tag{12}$$

where $R_j^n = \mathcal{O}(\tau^{4-\alpha} + h^8)$.

Similarly to the stability analysis, we define the grid functions $E^n(x)$ and $R^n(x)$:

$$E^n(x) = \sum_{l=-\infty}^{\infty} e_n(l)e^{i\beta x}, \quad \text{where} \quad e_n(l) = \frac{1}{L}\int_0^L E^n(x)e^{-i\beta x}dx, \quad \beta = \frac{2\pi l}{L} \quad \text{and} \quad i = \sqrt{-1},$$

$$R^n(x) = \sum_{l=-\infty}^{\infty} r_n(l)e^{i\beta x}, \quad \text{where} \quad r_n(l) = \frac{1}{L}\int_0^L R^n(x)e^{-i\beta x}dx, \quad \beta = \frac{2\pi l}{L} \quad \text{and} \quad i = \sqrt{-1}.$$

Assuming that $E_j^n = e_n e^{i\beta jh}$ and $R_j^n = r_n e^{i\beta jh}$ and subtracting them from Equation (12), we derive

$$\begin{aligned} & e_n\Big[\Big(\frac{\mu\lambda_0}{280} - \frac{q_j}{280} - \frac{\theta}{45}\Big)\cos(3\beta h) + \Big(-\frac{3\mu\lambda_0}{140} + \frac{3q_j}{140} + \frac{3\theta}{10}\Big)\cos(2\beta h) \\ & + \Big(\frac{3\mu\lambda_0}{56} - \frac{3q_j}{56} - 3\theta\Big)\cos(\beta h) + \Big(\frac{27\mu\lambda_0}{28} - \frac{27q_j}{28} + \frac{49\theta}{18}\Big)\Big] \\ & = -\mu\sum_{k=1}^{n-1}\lambda_k\Big(\frac{1}{280}\cos(3\beta h) - \frac{3}{140}\cos(2\beta h) + \frac{3}{56}\cos(\beta h) + \frac{27}{28}\Big)e_{n-k} \\ & \quad + \Big(\frac{1}{280}\cos(3\beta h) - \frac{3}{140}\cos(2\beta h) + \frac{3}{56}\cos(\beta h) + \frac{27}{28}\Big)r_n. \end{aligned}$$

It follows that

$$e_n = \sum_{k=1}^{n-1}\frac{-\mu\lambda_k B_1}{(\mu\lambda_0 - q_j)B_1 + \theta B_2}e_{n-k} + \frac{-\mu\lambda_k B_1}{(\mu\lambda_0 - q_j)B_1 + \theta B_2}r_n. \tag{13}$$

In preparation for the proof of Theorem 2, we first introduce some necessary definitions:

$$\|E^n\|^2 = h\sum_{j=1}^{M-1}|E_j^n|^2 = L\sum_{l=-\infty}^{\infty}|e_n(l)|^2, \tag{14}$$

$$\|R^n\|^2 = h\sum_{j=1}^{M-1}|R_j^n|^2 = L\sum_{l=-\infty}^{\infty}|r_n(l)|^2. \tag{15}$$

Theorem 2. *The numerical scheme given by Equation (5) converges with order* $\mathcal{O}(\tau^{4-\alpha} + h^8)$.

Proof. We begin by employing mathematical induction to demonstrate the existence of a positive constant C such that the following inequality holds for all $n \in [N]$:

$$|e_n| \le C|r_1|.$$

Since $R_j^n = \mathcal{O}(\tau^{4-\alpha} + h^8)$, by Equation (15), we can assert the existence of a positive constant C_n for each $n \in [N]$ such that

$$|r_n| \le C_n|r_1|.$$

When $n = 1$, according to Equation (13), we obtain

$$\begin{aligned} |e_1| &= \Big|\frac{-\mu\lambda_1 B_1}{(\mu\lambda_0 - q_j)B_1 + \theta B_2}r_1\Big| \\ &\le \Big|\frac{\mu\lambda_0 B_1}{(\mu\lambda_0 - q_j)B_1 + \theta B_2}\Big||r_1|, \end{aligned}$$

and, similar to Equation (10), we can derive

$$|e_1| \le C_1|r_1|.$$

Now, we assume that the inequality

$$|e_n| \le C_n|r_1|$$

holds for $n = 2, 3, \cdots, N-1$.

We define C' as the maximum value among the constants $\{C_1, C_2, \cdots, C_N\}$.

When $n = N$, according to Equation (13) and Lemma 3, we derive

$$\begin{aligned}
|e_N| &= \Big| \sum_{k=1}^{N-1} \frac{-\mu\lambda_k B_1}{(\mu\lambda_0 - q_j)B_1 + \theta B_2} e_{N-k} + \frac{B_1}{(\mu\lambda_0 - q_j)B_1 + \theta B_2} r_N \Big| \\
&\le \sum_{k=1}^{N-1} \Big| \frac{-\mu\lambda_k B_1}{(\mu\lambda_0 - q_j)B_1 + \theta B_2} \Big| |e_{N-k}| + \Big| \frac{B_1}{(\mu\lambda_0 - q_j)B_1 + \theta B_2} \Big| |r_N| \\
&\le \sum_{k=1}^{N-1} \Big| \frac{-\mu\lambda_k B_1}{(\mu\lambda_0 - q_j)B_1 + \theta B_2} \Big| C_{N-k}|r_1| + \Big| \frac{B_1}{(\mu\lambda_0 - q_j)B_1 + \theta B_2} \Big| C_N|r_1| \\
&\le C' \Big| \frac{\mu\tau^{-\alpha} B_1}{(\mu\tau^{-\alpha}\psi_0 - q_j)B_1 + \theta B_2} \Big| (\psi_0 + 2\psi_2)|r_1| + C' \Big| \frac{B_1}{(\mu\tau^{-\alpha}\psi_0 - q_j)B_1 + \theta B_2} \Big| |r_1| \\
&\le C'(1 + \psi_0 + 2\psi_2)|r_1| \\
&\le C|r_1|.
\end{aligned}$$

Then, by Equation (14) and (15), we obtain

$$\begin{aligned}
\|E^n\|^2 &= L \sum_{l=-\infty}^{\infty} |e_n(l)|^2 \\
&\le L \sum_{l=-\infty}^{\infty} C^2 |r_1(l)|^2 \\
&= C^2 \|R^1\|^2 \\
&\le C^2 (\tau^{4-\alpha} + h^8)^2.
\end{aligned}$$

Therefore, the numerical scheme given by Equation (5) converges with order $\mathcal{O}(\tau^{4-\alpha} + h^8)$. □

4. Numerical Results

Our innovative high-order scheme for time-fractional CDREs with variable coefficients was rigorously validated through computational experiments, which revealed its convergence order and confirmed its effectiveness. All numerical experiments were conducted using MATLAB 2020b. The errors E_1 and E_2 were computed with mesh sizes h_1 and h_2, respectively, and the errors and convergence rates were quantified as follows:

$$L^\infty\text{-Error} = \max_{1 \le n \le N} |u^n - U^n|, \quad L^\infty\text{-Rate} = log(E_1/E_2)/log(h_1/h_2).$$

To rigorously validate the accuracy and robustness of our proposed method, we compared its results against known analytical solutions under controlled conditions in Examples 1–3.

Example 1. *We examine Equation (2) in the domain* $[0,2] \times [0,1]$ *with* $d = 1$, $p_1(x) = \frac{1}{1+x}$, $p_2(x) = x^2$, *and* $f(x,t) = \left(\frac{\Gamma(5+\alpha)}{24} - t^\alpha x^2\right) t^4 (1+x)^2$. *The exact solution is* $v(x,t) = t^{4+\alpha}(1+x)^2$.

To validate our approach, we compare our results with those in [21]. Table 1 shows a comparison of the error and temporal convergence rates between our method and that in [21] under different N values and α values with $M = 100$. Similarly, Table 2 compares the error and spatial convergence rates between our method and that in [21] under different M values and α values (where N = 15,000 in [21], and $N = \lfloor (\frac{M}{2})^{\frac{8}{4-\alpha}} \rfloor$ in our method). These comparisons clearly demonstrate the advantages of our approach. Figure 1 visually presents the exact solution, numerical solution, absolute error, and error contour plot when $\alpha = 0.01$, $M = 100$, and $N = 100$, further validating the accuracy and convergence of our method. Together, these results provide a solid foundation for validating our approach and demonstrate its effectiveness and reliability under various parameter settings.

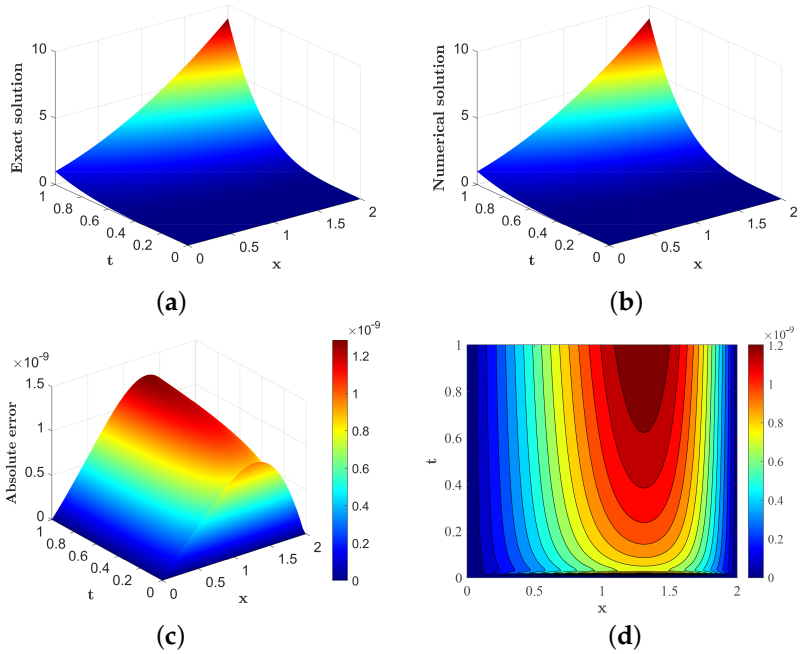


Figure 1. Visualization of Example 1 with $\alpha = 0.01$, $M = 100$, and $N = 100$: (**a**) exact solution; (**b**) numerical solution; (**c**) absolute error; (**d**) contour plot of error.

Table 1. Comparison of error and temporal convergence rates for Example 1 at $M = 100$.

	N	$\alpha = 0.25$		$\alpha = 0.5$		$\alpha = 0.75$	
		L^∞-Error	L^∞-Rate	L^∞-Error	L^∞-Rate	L^∞-Error	L^∞-Rate
[21]	40	2.5734×10^{-5}	—	8.3385×10^{-5}	—	1.9864×10^{-4}	—
	80	3.2434×10^{-6}	2.9881	1.0540×10^{-5}	2.9839	2.5199×10^{-5}	2.9787
	160	4.0709×10^{-7}	2.9941	1.3249×10^{-6}	2.9920	3.1730×10^{-6}	2.9894
	320	5.0989×10^{-8}	2.9971	1.6607×10^{-7}	2.9960	3.9807×10^{-7}	2.9947
Our	40	3.8755×10^{-6}	—	3.0304×10^{-5}	—	1.7518×10^{-4}	—
	80	2.9991×10^{-7}	3.6918	2.7402×10^{-6}	3.4672	1.8793×10^{-5}	3.2206
	160	2.2996×10^{-8}	3.7051	2.4561×10^{-7}	3.4798	1.9964×10^{-6}	3.2347
	320	1.7106×10^{-9}	3.7488	2.1851×10^{-8}	3.4906	2.1095×10^{-7}	3.2424

Table 2. Comparison of error and spatial convergence rates for Example 1.

	M	$\alpha = 0.25$		$\alpha = 0.5$		$\alpha = 0.75$	
		L^∞-Error	L^∞-Rate	L^∞-Error	L^∞-Rate	L^∞-Error	L^∞-Rate
[21]	8	7.1868×10^{-8}	—	5.6976×10^{-8}	—	4.4166×10^{-8}	—
	16	4.5156×10^{-9}	3.9924	3.5806×10^{-9}	3.9921	2.7763×10^{-9}	3.9917
	32	2.8239×10^{-10}	3.9992	2.2351×10^{-10}	4.0018	1.7308×10^{-10}	4.0036
	64	1.7339×10^{-11}	4.0255	1.3457×10^{-11}	4.0539	1.0351×10^{-11}	4.0635
Our	8	1.0969×10^{-2}	—	3.4659×10^{-2}	—	6.6072×10^{-2}	—
	16	5.9367×10^{-5}	7.5295	1.7548×10^{-4}	7.6258	4.3821×10^{-4}	7.2363
	32	2.5068×10^{-7}	7.8877	7.5292×10^{-7}	7.8646	1.7378×10^{-6}	7.9782
	64	1.0027×10^{-9}	7.9658	3.0181×10^{-9}	7.9627	6.2153×10^{-9}	8.1273

Example 2. *We examine Equation (2) with the following parameter settings:* $d = 1$, $p_1(x) = -\sin x$, $p_2(x) = -\cos x$, *and* $f(x,t) = \frac{\Gamma(5+\alpha)}{24} t^4 \cos x + t^{4+\alpha}(1 + \cos x)$. *The exact solution for validation purposes is given by* $v(x,t) = t^{4+\alpha} \cos x$.

Table 3 presents a detailed comparison of the error and temporal convergence rates for Example 2 with different α values, directly comparing our results with those in [21]. Table 4 presents the error and spatial convergence rates for Example 2 under different M values and α values with $N = \lfloor (\frac{M}{2})^{\frac{8}{4-\alpha}} \rfloor$. This analysis is conducted over the domain $[0, \pi] \times [0, 1]$, highlighting the effectiveness of our method against established results. For plotting and visualization purposes, we employ a different region, $[0, 6\pi] \times [0, 1]$, to better highlight the specific features of the solution. This extended domain allows us to observe the periodic nature of the solution more clearly by capturing multiple periods, providing valuable insights into the long-term behavior and periodicity. Additionally, it helps in understanding the boundary effects and their influence on the solution, which is particularly important when boundary conditions significantly impact the overall behavior.

Table 3. Comparison of error and temporal convergence rates for Example 2 with different α values.

	$M \times N$	$\alpha = 0.25$		$\alpha = 0.5$		$\alpha = 0.75$	
		L^∞-Error	L^∞-Rate	L^∞-Error	L^∞-Rate	L^∞-Error	L^∞-Rate
[21]	1000×40	2.7763×10^{-6}	—	9.0510×10^{-6}	—	2.1821×10^{-5}	—
	1000×80	3.4991×10^{-7}	2.9881	1.1439×10^{-6}	2.9841	2.7671×10^{-6}	2.9793
	1000×160	4.3916×10^{-8}	2.9941	1.4378×10^{-7}	2.9921	3.4835×10^{-7}	2.9897
	1000×320	5.4995×10^{-9}	2.9974	1.8021×10^{-8}	2.9961	4.3698×10^{-8}	2.9949
Our	200×40	4.1605×10^{-7}	—	3.2513×10^{-6}	—	1.8881×10^{-5}	—
	200×80	3.2193×10^{-8}	3.6920	2.9393×10^{-7}	3.4675	2.0243×10^{-6}	3.2215
	200×160	2.4677×10^{-9}	3.7055	2.6341×10^{-8}	3.4801	2.1497×10^{-7}	3.2352
	200×320	1.8287×10^{-10}	3.7543	2.3426×10^{-9}	3.4911	2.2711×10^{-8}	3.2427

Table 4. Error and spatial convergence rates for Example 2 with different α values and $N = \lfloor (\frac{M}{2})^{\frac{8}{4-\alpha}} \rfloor$.

M	$\alpha = 0.25$		$\alpha = 0.5$		$\alpha = 0.75$	
	L^∞-Error	L^∞-Rate	L^∞-Error	L^∞-Rate	L^∞-Error	L^∞-Rate
16	2.2560×10^{-4}	—	7.8067×10^{-4}	—	1.5142×10^{-3}	—
24	9.3857×10^{-6}	7.8418	2.9720×10^{-5}	8.0607	6.6303×10^{-5}	7.7157
32	9.3441×10^{-7}	8.0193	2.9686×10^{-6}	8.0079	6.7649×10^{-6}	7.9340
40	1.5472×10^{-7}	8.0589	4.8711×10^{-7}	8.0995	1.1578×10^{-6}	7.9106

Figure 2 uses the larger domain $[0, 6\pi] \times [0, 1]$ to illustrate the exact solution, numerical solution, absolute error, and error contour plot for $\alpha = 0.99$, $M = 200$, and $N = 100$. These visualizations further validate the accuracy and convergence of our method under these conditions.

Example 3. *We examine Equation (2) in the domain* $[0, \pi] \times [0, 2]$ *with* $d = 1$, $p_1(x) = -1$, $p_2(x) = 1$, *and* $f(x,t) = \frac{\Gamma(5+\alpha)}{24} t^4 \cos x + t^{4+\alpha} \sin x$. *The exact solution for validation purposes is given by* $v(x,t) = t^{4+\alpha} \cos x$.

In this final example, we switch to constant coefficients to consolidate our findings from Examples 1 and 2, which deal with variable coefficients. This allows us to reinforce the reliability and robustness of our method across different types of coefficient settings. Table 5 presents the L^∞-error and convergence rates for temporal and spatial discretizations at $\alpha = 0.5$. For brevity, we focus on $\alpha = 0.5$, though our findings generalize to other α values. This table illustrates the method's performance under different grid resolutions, demonstrating the expected convergence behavior. Table 6 compares the numerical solutions (v_n) and exact solutions (v_e) for different α values and grid points at $T = 2$. This comparison provides a direct assessment of the numerical solution's accuracy across various

parameter settings. Figure 3 provides a visual convergence analysis with different α values: (a) $log(Error)$ vs. $log(\tau)$ for temporal convergence and (b) $log(Error)$ vs. $log(h)$ for spatial convergence. These plots further validate the method's effectiveness and convergence properties for a range of α values, serving as a solid conclusion to our series of examples.

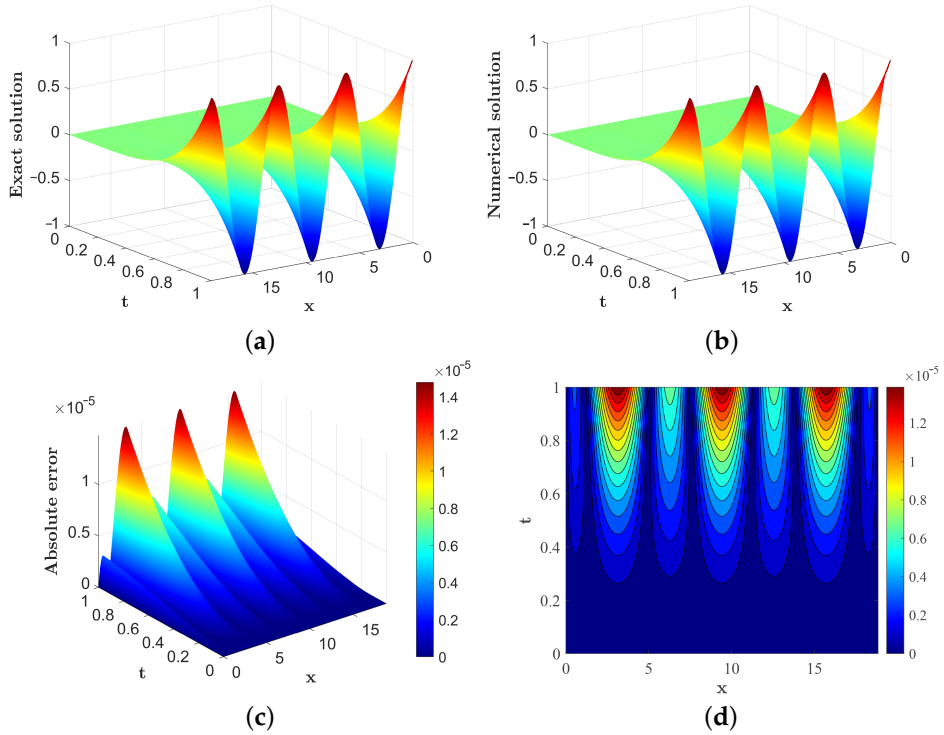


Figure 2. Visualization of Example 2 with $\alpha = 0.99$, $M = 200$, and $N = 100$: (**a**) exact solution; (**b**) numerical solution; (**c**) absolute error; (d) contour plot of error.

Table 5. L^{∞}-error and temporal/spatial convergence rates for Example 3 at $\alpha = 0.5$.

Temporal Convergence			Spatial Convergence		
$M \times N$	L^{∞}-Error	L^{∞}-Rate	$M \times N$	L^{∞}-Error	L^{∞}-Rate
100×10	7.4329×10^{-3}	—	10×1000	3.4979×10^{-4}	—
100×20	7.0324×10^{-4}	3.4018	15×1000	1.4734×10^{-5}	7.8112
100×40	6.4632×10^{-5}	3.4437	20×1000	1.4621×10^{-6}	8.0308
100×80	5.8474×10^{-6}	3.4664	25×1000	2.4045×10^{-7}	8.0893

Table 6. Comparison of numerical solutions (v_n) and exact solutions (v_e) for Example 3.

x	$\alpha = 0.01$		$\alpha = 0.5$		$\alpha = 0.99$	
	v_n	v_e	v_n	v_e	v_n	v_e
$\frac{\pi}{8}$	14.88488997	14.88488997	20.90500831	20.90500744	29.35998710	29.35993057
$\frac{2\pi}{8}$	11.39240157	11.39240156	16.00000041	16.00000000	22.47115654	22.47111801
$\frac{3\pi}{8}$	6.16552330	6.16552330	8.65913689	8.65913760	12.16126336	12.16128143
$\frac{4\pi}{8}$	0.00000000	0.00000000	−0.00000188	0.00000000	−0.00008026	0.00000000
$\frac{5\pi}{8}$	−6.16552330	−6.16552330	−8.65914020	−8.65913760	−12.16140299	−12.16128143
$\frac{6\pi}{8}$	−11.39240157	−11.39240156	−16.00000257	−16.00000000	−22.47124269	−22.47111801
$\frac{7\pi}{8}$	−14.88488997	−14.88488997	−20.90500912	−20.90500744	−29.36001345	−29.35993057

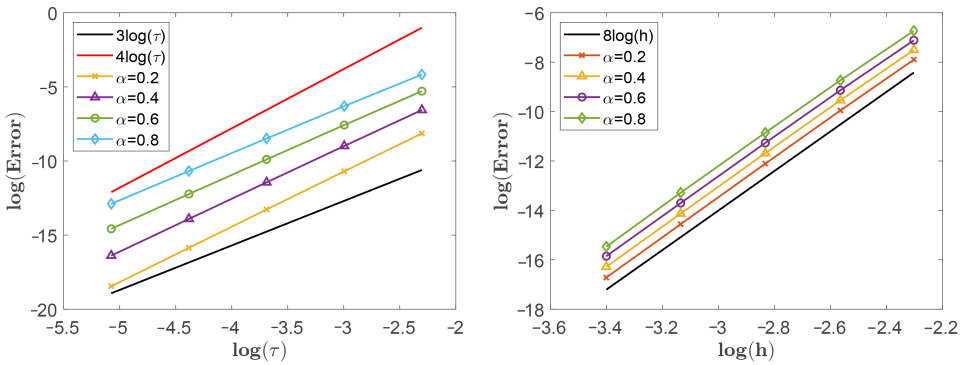


Figure 3. Convergence analysis with different α values: (**a**) log(*Error*) vs. log(τ) for temporal convergence; (**b**) log(*Error*) vs. log(h) for spatial convergence.

5. Conclusions

In conclusion, we develop a novel numerical scheme for time-fractional CDREs with variable coefficients that combines Lagrange polynomial interpolation for time discretization with a compact finite difference approximation for spatial derivatives. The proposed method exhibits unconditional stability and achieves high-order convergence rates, reaching $4-\alpha$-order accuracy in time and eighth-order accuracy in space, as rigorously verified through a Fourier analysis. These results represent a substantial improvement in the numerical solution of fractional partial differential equations. Numerical results validate our theoretical analysis, demonstrating the superior accuracy and efficiency of our method over existing solutions. The present study focuses on 1D problems to establish the foundational accuracy and convergence properties of our method. While this simplifies validation, we acknowledge that extensions to 2D/3D or more complex geometries will require further development, particularly in computational efficiency and boundary condition handling. Additionally, our tests primarily involve linear problems. Application to nonlinear CDREs or real-world scenarios remains a challenge for us. Future work may also explore adaptive mesh strategies and the incorporation of nonlinearity in spatial operators for more realistic modeling.

Author Contributions: Conceptualization, Y.F.; software, Y.F. and L.W.; formal analysis, Y.F. and X.Z.; writing—original draft preparation, Y.F.; writing—review and editing, X.Z. and L.W.; visualization, Y.F. and L.W. All authors have read and agreed to the published version of the manuscript.

Funding: This research was funded by the Scientific Research Foundation for Talents Introduction of Guizhou University of Finance and Economics (No. 2023YJ16); the Institute of Complexity Science, Henan University of Technology (No. CSKFJJ-2025-33); and the Henan Provincial International Science and Technology Cooperation Project (No. 252102520007).

Data Availability Statement: The data analyzed in this study are subject to the following licenses/restrictions: the first author can receive the restrictions. Requests to access these datasets should be directed to fyl001215@163.com (Y. L. Feng).

Acknowledgments: The authors are very grateful to the referee for carefully reading the article and providing many valuable comments.

Conflicts of Interest: The authors declare no conflicts of interest.

References

1. Almeida, R.; Bastos, N.R.O.; Monteiro, M.T.T. Modeling some real phenomena by fractional differential equations. *Math. Method. Appl. Sci.* **2016**, *39*, 4846–4855.
2. Zhang, Y.; Sun, H.G.; Stowell, H.H.; Zayernouri, M.; Hansen, S.E. A review of applications of fractional calculus in Earth system dynamics. *Chaos Soliton. Fract.* **2017**, *102*, 29–46.
3. Failla, G.; Zingales, M. Advanced materials modelling via fractional calculus: Challenges and perspectives. *Philos. Trans. R. Soc. A.* **2020**, *378*, 2172.
4. Duran, S.; Durur, H.; Yavuz, M.; Yokus, A. Discussion of numerical and analytical techniques for the emerging fractional order Murnaghan model in materials science. *Opt. Quant. Electron.* **2023**, *55*, 571.
5. Toledo-Hernandez, R.; Rico-Ramirez, V.; Iglesias-Silva, G.A.; Diwekar, U.M. A fractional calculus approach to the dynamic optimization of biological reactive systems. Part I: Fractional models for biological reactions. *Chem. Eng. Sci.* **2014**, *117*, 217–228.
6. Ali, K.K.; Mohamed, M.S.; Maneea, M. Unveiling the dynamics of plasma dilution in medical science through analytical and numerical approaches via fractional integro-differential equations. *J. Appl. Math. Comput.* **2025**, *71*, 1219–1245.
7. Das, P.; Mehrmann, V. Numerical solution of singularly perturbed convection-diffusion-reaction problems with two small parameters. *BIT Numer. Math.* **2016**, *56*, 51–76.
8. Giere, S.; Iliescu, T.; John, V.; Wells, D. SUPG reduced order models for convection-dominated convection-diffusion-reaction equations. *Comput. Method. Appl. M.* **2015**, *289*, 454–474.
9. Chen, G.; Feng, M.F.; Xie, X.P. A robust WG finite element method for convection-diffusion-reaction equations. *J. Comput. Appl. Math.* **2017**, *315*, 107–125.
10. Lin, R.C.; Ye, X.; Zhang, S.Y.; Zhu, P. A Weak Galerkin Finite Element Method for Singularly Perturbed Convection-Diffusion-Reaction Problems. *SIAM J. Numer. Anal.* **2018**, *56*, 1482–1497.
11. Xu, M.T. A modified finite volume method for convection-diffusion-reaction problems. *Int. J. Heat Mass Transf.* **2018**, *117*, 658–668.
12. Zhang, X.D.; Feng, Y.L.; Luo, Z.Y.; Liu, J. A spatial sixth-order numerical scheme for solving fractional partial differential equation. *Appl. Math. Lett.* **2025**, *159*, 109265.
13. Feng, Y.L.; Zhang, X.D.; Chen, Y.; Wei, L.L. A compact finite difference scheme for solving fractional Black-Scholes option pricing model. *J. Inequal. Appl.* **2025**, *2025*, 36.
14. Li, C.P.; Wang, Z. Numerical methods for the time fractional convection-diffusion-reaction equation. *Numer. Func. Anal. Opt.* **2021**, *42*, 1115–1153.
15. Ngondiep, E. A two-level fourth-order approach for time-fractional convection-diffusion-reaction equation with variable coefficients. *Commun. Nonlinear Sci.* **2022**, *111*, 106444.
16. Roul, P.; Rohil, V. An efficient numerical scheme and its analysis for the multiterm time-fractional convection-diffusion-reaction equation. *Math. Method. Appl. Sci.* **2023**, *46*, 16857–16875.
17. Hosseini, V.R.; Mehrizi, A.A.; Karimi-Maleh, H.; Naddafi, M. A numerical solution of fractional reaction-convection-diffusion for modeling PEM fuel cells based on a meshless approach. *Eng. Anal. Bound. Elem.* **2023**, *155*, 707–716.
18. Priyadarshana, S.; Mohapatra, J. An efficient fractional step numerical algorithm for time-delayed singularly perturbed 2D convection-diffusion-reaction problem with two small parameters. *Numer. Algorithms* **2024**, *97*, 687–726.
19. Kumar, N.; Toprakseven, S.; Jiwari, R. A numerical method for singularly perturbed convection-diffusion-reaction equations on polygonal meshes. *Comput. Appl. Math.* **2024**, *43*, 44.
20. Liu, M.M.; Zheng, X.C.; Li, K.X.; Qiu, W.L. High-order compact difference method for convection-reaction-subdiffusion equation with variable exponent and coefficients. *Numer. Algorithms* **2025**. [CrossRef]
21. Ren, L.; Wang, Y.M. A fourth-order extrapolated compact difference method for time-fractional convection-reaction-diffusion equations with spatially variable coefficients. *Appl. Math. Comput.* **2017**, *312*, 1–22.
22. Abdi, N.; Aminikhah, H.; Refahi Sheikhani, A.H. High-order compact finite difference schemes for the time-fractional Black-Scholes model governing European options. *Chaos Soliton. Fract.* **2022**, *162*, 112423.
23. Kumari, S.; Singh, A.K.; Mehandiratta, V.; Mehra, M. High-order approximation to Caputo derivative on graded mesh and time-fractional diffusion equation for nonsmooth solutions. *J. Comput. Nonlin. Dyn.* **2024**, *19*, 10.

Disclaimer/Publisher's Note: The statements, opinions and data contained in all publications are solely those of the individual author(s) and contributor(s) and not of MDPI and/or the editor(s). MDPI and/or the editor(s) disclaim responsibility for any injury to people or property resulting from any ideas, methods, instructions or products referred to in the content.